Chapter 16

What Can We Learn from a Small Regulatory Membrane Protein?

Gianluigi Veglia, Kim N. Ha, Lei Shi, Raffaello Verardi, and Nathaniel J. Traaseth

Abstract

This chapter reviews the molecular biology, biochemical, and NMR methods that we used to study the structural dynamics, membrane topology, and interaction of phospholamban (PLN), a small regulatory membrane protein involved in the regulation of the sarcoplasmic reticulum Ca-ATPase (SERCA). In particular, we show the progression of our research from the initial hypotheses toward understanding the molecular mechanisms of SERCA's regulation, including the effects of PLN oligomerization and post-translational phosphorylation. Finally, we show how the knowledge of the molecular mechanism of the structural dynamics and topology of free and bound proteins can lead to the rational design of PLN analogs for possible use in gene therapy.

Key words: Phospholamban, SERCA, Ca-ATPase, Structural dynamics, Topology, Membrane proteins, NMR, PISEMA

1. Introduction

Phospholamban (PLN) is a small integral membrane protein (52 residues) localized in the sarcoplasmic reticulum (SR) membrane that regulates the flow of calcium ions into the SR lumen of cardiac muscle (1). Specifically, PLN binds to SR calcium ATPase (SERCA), the enzyme responsible for calcium re-uptake into the SR lumen. In its unphosphorylated form, PLN inhibits SERCA by reducing its affinity for calcium. Upon β-adrenergic stimulation, PLN is phosphorylated by protein kinase A at S16 with concomitant relief of SERCA inhibition and restoration of SERCA activity. These cyclic events account for the relaxation (diastolic phase) of the heart muscle, which if disrupted, may evolve into heart

Jean-Jacques Lacapère (ed.), *Membrane Protein Structure Determination: Methods and Protocols*, Methods in Molecular Biology, vol. 654, DOI 10.1007/978-1-60761-762-4_16,

failure (2). Due to their central role in cardiac muscle contractility, PLN and SERCA have become targets for new, alternative therapies for heart failure (3). What can be learned from the study of the structural and dynamic transitions of PLN free and bound to SERCA?, More importantly, can these studies contribute in the development of new clinical approaches to heart failure?

Much progress has been made toward understanding the molecular mechanism of SERCA within the enzymatic cycle (4, 5). Chapters 9 and 15 of this volume give exquisite portraits of the latest findings, outlining the successes of x-ray crystallography in reconstructing the structural transitions of SERCA during enzyme turnover. Undeniably, the first crystal structure of SERCA (E1-Ca_2, calcium-bound form) solved by Toyoshima and co-workers paved the way for the atomic level understanding of calcium translocation in the SR (6). To date, there are several crystal structures of SERCA under different experimental conditions that are allowing enzymologists to model the major conformational states of the enzyme during turnover (7). However, very few studies have been dedicated to the determination of the complexes between SERCA and its endogenous inhibitor PLN. This is probably due to the inherent dynamics of the SERCA/PLN complex that might complicate the formation of large, diffracting crystals. This hypothesis is reinforced by several fluorescence and EPR studies published by the Thomas and Squier Laboratories underscoring the dynamic nature of the SERCA/PLN complex (8–14). So far, the labs of Stokes and Young (15, 16) have produced the best images of this complex although the quality of the crystals does not define the interaction surface between the two proteins at the atomic level. NMR studies, on the other hand, have been focused on the structural dynamics of PLN in the unbound form. This is mainly due to the difficulties in producing isotopically labeled SERCA and analyzing its complex with PLN by solution-state NMR (M_w ~ 116 kDa).

Our laboratory, in collaboration with the Thomas laboratory, has used a combination of solution and solid-state NMR methods to map the structural dynamics, topology, and interactions between PLN and SERCA. Based on our chemical shift perturbation data from solution NMR, we have constructed an allosteric model for SERCA regulation by PLN (11, 13, 17–19). This regulatory model has been now adopted by several groups in the fields of structural biology and muscle physiology to explain the effects of naturally occurring and engineered mutations in PLN. More importantly, this model has allowed us to rationally manipulate the structural dynamics of PLN and design new mutants that are possible candidates for gene therapy in heart failure treatment.

In the following sections, we briefly review the molecular biology, biochemistry, and NMR approaches that we have used to study SERCA's regulation by looking at PLN free (monomeric

and pentameric) and bound to SERCA. We show the progression of our research from our initial hypotheses on the mechanism of SERCA regulation by PLN to our initial attempts to control PLN structural dynamics to tune SERCA's function.

2. Materials

2.1. Expression and Purification of Monomeric and Pentameric PLN

2.1.1. Plasmid Construction and Mutagenesis of AFA–PLN

1. pMal c2E maltose-binding protein vector (New England Biolabs, Ipswich, MA).
2. Oligonucleotide primers (Biomedical Genomics Center, University of MN).
3. Pfu Turbo DNA polymerase (Stratagene, La Jolla, CA).
4. dNTP mix (Promega, Madison, WI).
5. T4 DNA ligase (Promega, Madison, WI).
6. 1× Luria–Bertani (LB) media.
7. Qiaprep Spin Miniprep Kit (Qiagen, Valencia, CA).

2.1.2. Expression of Unlabeled and ^{15}N Uniformly Labeled PLN

1. BL21(DE3) strain *E. coli* cells (Novagen, Gibbstown, NJ).
2. 1× Luria–Bertani broth media.
3. M9 minimal media containing 12.8 g/L $Na_2HPO_4{\cdot}7H_2O$, 3 g/L KH_2PO_4, 0.5 g/L NaCl, and 1 g/L ^{15}N-labeled NH_4Cl, 2 g/L glucose, and 0.1% w/v ampicillin.
4. 1 M IPTG (Gold Biotechnology, St. Louis, MO).
5. Mineral cocktail: 6 mg/L $CaCl_2$, 6 mg/L $FeSO_4$, 1 mg/L $MnCl_2$, 0.8 mg/L $CoCl_2$, 0.7 mg/L $ZnSO_4$, 0.3 mg/L $CuCl_2$, 0.02 mg/L H_3BO_3, 0.25 mg/L $(NH_4)_6MO_7O_{24}$, and 5 mg/L EDTA.
6. Vitamin cocktail: 1 mg/L calcium pentothenate, 1 mg/L biotin, 1 mg/L folic acid, 1 mg/L niacinamide, and 1 mg/L pyridoxal phosphate.

2.1.3. Purification of PLN

1. Lysis buffer: 20 mM PBS pH 7.3, 120 mM NaCl, 8 mM EDTA, 0.1 mM DTT, 52.6 mM glycerol, 0.5 μg/mL pepstatin A, 0.5 μg/mL leupeptin, 2.5 μM lysozyme, and 4.5 mM Tween-20.
2. Amylose affinity chromatography resin (New England Biolabs, Ipswich, MA).
3. Wash buffer: 20 mM PBS pH 7.3, 120 mM NaCl.
4. Maltose elution buffer: 46 mM maltose in 20 mM PBS pH 7.3, 120 mM NaCl, 1 mM EDTA, and 3.1 mM NaN_3.
5. Recombinant tobacco etch virus serine protease (Invitrogen, Carlsbad, CA or expressed and purified in our own lab) (see Note 2).

6. Dialysis membranes with 1,000-kDa molecular weight cutoff.
7. HPLC purification: H_2O with 0.1% trifluoroacetic acid and isopropanol.

2.1.4. Quantification

1. Bio-Rad gradient 10–15% polyacrylamide gel (Bio-Rad, Hercules, CA).
2. Protein standard.

2.1.5. Phosphorylation of PLN at S16 by cAMP-Dependent Protein Kinase A

1. Phosphorylation buffer: 20 mM MOPS (pH 7.3), 1% β-Octylglucoside, 1 mM ATP, and 1 mM $MgCl_2$.
2. cAMP-dependent protein kinase A catalytic subunit (Sigma) or recombinant kinase as described in ref. 20.

2.2. SERCA Preparation

1. White muscle from the back and hind legs of rabbit.
2. Extraction buffer: 20 mM MOPS and 0.1 M KCl, pH 7.
3. Sucrose buffer: 20 mM MOPS, 0.3 M sucrose, 1 mM NaN_3.
4. Reactive red affinity resin (Sigma).
5. SERCA buffer: 5 mM DPC, 1 mM $CaCl_2$, 1 mM $MgCl_2$, 20 mM MOPS (pH 7.0), 20% glycerol, 0.25 mM DTT, and 4 mM ADP.

2.3. Functional Assays

2.3.1. SERCA PLN Co-reconstitution

1. 1,2-Dioleoyl-*sn*-glycero-3-phosphocholine (DOPC) and 1,2-dioleoyl-*sn*-glycero-phosphoethanolamine (DOPE) (Avanti Polar Lipids, Alabaster, AL).
2. Biobeads (Bio-Rad, Hercules, CA).
3. β-Octylglucoside (Sigma).

2.3.2. ATPase Activity Measurements

1. Coupled enzyme assay mix containing 0.5 mM phosphoenol pyruvate, 2.5 mM ATP, 0.2 mM NADH, 2 IU of pyruvate kinase, 2 IU of lactate dehydrogenase, and 1–2 μg calcium ionophore (A23187).

2.3.3. ^{31}P NMR Activity Assays

1. Coupled enzyme assay mix containing a final concentration of 10 mM dodecylphosphocholine, 1 mM $MgCl_2$, 80 mM ATP, 20 mM MOPS (pH 7.0), and 0.2% $C_{12}E_8$.

2.4. NMR Spectroscopy

2.4.1. Solution-State Samples for Titration

1. Dodecylphosphocholine (DPC) (Avertec or Cambridge Isotope Laboratories).
2. Solution-state NMR sample buffer containing 20 mM Na_2PO_4, 120 mM NaCl, and 0.1% NaN_3.
3. Mini-dialysis chambers (Millipore, Billerica, MA).
4. Guanidinium–HCl (Sigma).
5. Dialysis buffer: 20 mM PBS and 50 mM β-mercaptoethanol.

2.4.2. Oriented Samples and ssNMR Spectroscopy

1. 10% (w/v) sodium dodecyl sulfate (SDS).
2. DOPC and DOPE lipids.
3. Ultra filtration concentrator (Amicon, Millipore Corporation, Bedford, MA).
4. Glass plates, 8×12 mm (Marienfeld GmbH & Co, Lauda-Konigshofen, Germany).
5. Trifluoroethanol.
6. Extruder (Northern Lipids Inc. Burnaby, BC, Canada).

3. Methods

3.1. Expression and Purification of Monomeric and Pentameric PLN

For structural studies of membrane proteins by NMR, it is necessary to find a robust expression system that allows for the purification of milligram quantities of pure protein. For this purpose, we optimized a fusion protein construct for both monomeric (cysteine null PLN with the following mutations C36A, C41F, and C46A, which we refer to as AFA–PLN) and pentameric species (21).

3.1.1. Construction of PLN and Mutant PLN Expression Plasmids

To maximize the expression, all of the codons were optimized for *E. coli*. The nucleic acid sequence was divided into four overlapping primers and three polymerase chain reactions (PCRs) were performed, with incorporation of a TEV protease cleavage site between MBP and PLN, an *Eco*RI restriction site at the 5′ end, and a *Hind*III site at the 3′ end (a map of the plasmid is available from ref. 21). Each PCR was performed with a total volume of 50 µL containing 0.06 µM of each oligonucleotide, 80 µg of parental template, 200 µM dNTP mix, and 5.0 U Pfu Turbo DNA polymerase. Each PCR was carried out in an Eppendorf Master Cycler system with standard temperature cycling suggested for Pfu Turbo DNA polymerase. AFA–PLN PCR product was amplified and then ligated into *Eco*RI and *Hind*III sites on the pMal c2E vector using T4 DNA ligase (Rationale for fusion partner is described in Note 1). The ligated product was used to transform XL1-Blue competent cells with transformants selected by growth on LB/ampicillin plates. For single-site mutations of PLN, the forward and reverse primers were designed with optimized codons for *E. coli* three residues before and after the target residue to be mutated. PCR was performed with Pfu DNA polymerase using the protocol described above. PCR products were then digested with Dpn-I in order to remove nonmutated methylated dsDNA and then were transformed into XL-Blue competent cells. Constructs were amplified and extracted using the Qiaquick Spin Miniprep kit.

3.1.2. PLN Expression

E. coli BL21(DE3) cells were transformed with MBP–PLN fusion constructs. One hundred milliliters of LB growth media with

50 μg/mL ampicillin was inoculated with a single colony and grown ~16 h at 25°C shaking at 250 rpm to reach an OD_{600} of ~1.0. The growth was then diluted (1:50) into M9 media containing mineral and vitamin cocktails and grown at 37°C to an OD_{600} of ~1.0. Protein expression was induced with 1 mM IPTG for 4.5 h at 37°C. All cells were harvested by centrifugation at 6,370 × *g* for 20 min at 4°C. Pellets were stored at −20°C.

3.1.3. PLN Purification

PLN pellets (~10–15 g) were resuspended in ~400 mL of lysis buffer and blended using a Sorval Omni-Mixer 17105. Cell lysates were then sonicated on ice for 15 min using a Branson Sonifier 450 sonicator at an output setting of 4 and a duty cycle of 45%. After sonication, lysates were spun down at 45,700 × *g* for 20 min at 4°C. The supernatant containing MBP/PLN fusion protein was applied to an amylose resin affinity chromatography column at 4°C. The column was washed with 12 column volumes of wash buffer until the OD_{280} was <0.05. The protein was eluted using a maltose solution, which MBP preferentially binds, releasing the protein from the amylose resin. PLN was cleaved from MBP with TEV protease at 100 U/mg fusion protein at 30°C for ~5–8 h. At this point, PLN can be further purified in two ways: (1) an S-100 sephacryl gel filtration column using an AKTA*prime* liquid chromatography system (Amersham Pharmacia Biotech) or (2) using reversed-phased HPLC. While we originally used the gel filtration method, we have abandoned this method in favor of the faster and higher resolving HPLC method as reported by Young and co-workers (22). For the HPLC method, the cleavage reaction was dialyzed against 4 L of ddH_2O in a 1,000-Da cutoff membrane until PLN precipitated (~12 h). The suspension was centrifuged at 6,370 × *g* for 20 min at 4°C. The supernatant containing soluble proteins (MBP, TEV protease, uncleaved fusion protein) was discarded. Pellets were solubilized in 1–2 mL of 10% (w/v) SDS and stored at 4°C. This crude solution was purified by reversed phase HPLC using an Agilent 1100 system (Agilent Technologies, Inc. Santa Clara, CA, USA) equipped with a Vydac 208TP C8 monomeric reversed phase column (250 × 1.0 mm i.d. ×10 μm particle size, Grace Vydac, Hesperia, CA, USA). The mobile phases used were: A – H_2O with 0.1% TFA and B – isopropanol. The column (incubated at 50°C) was equilibrated with 10% solvent B and proteins were eluted at 2 mL/min flow rate using the following gradient: 10–30% solvent B in 10 min, 30–50% in 20 min, 50–70% in 30 min, and 70–100% in final 10 min. The column was re-equilibrated with 10% B for 10 min after each run. With these conditions, the retention time for PLN was ~59 min. PLN fractions were pooled and isopropanol was evaporated under a stream of N_2. The resulting suspension was lyophilized and stored at −20°C.

3.1.4. Quantification of Protein

Protein concentration at each purification step was determined using protein absorbance at 280 nm, or assayed with densitometry measurements of Coomassie or silver stained gels (Fig. 1a). Densitometry data was collected on a Bio-Rad Molecular Imager FX using Bio-Rad Quantity One quantitation software. Recombinant protein concentrations were determined by comparison to a standard curve of 1–3 μg synthetic PLN peptides previously quantified by amino acid analysis. PLN was also identified with MALDI-TOF MS and amino acid sequence analysis.

3.1.5. Phosphorylation of PLN at S16 by PKA

HPLC-purified PLN was reconstituted to a concentration of 0.25 mg/mL for phosphorylation. One milligram PLN was phosphorylated with 1,000 U of protein kinase A catalytic subunit. Phosphorylation was confirmed using a gel-shift from a Western blot with anti-pS16 PLN antibody 285 and by MALDI-TOF MS.

3.2. SERCA Preparation

SERCA was extracted from rabbit skeletal muscle, purified, and tested for activity as reported previously (15, 17, 18). A solution containing 0.45 mM of SERCA, 5 mM DPC, 1 mM $CaCl_2$, 1 mM $MgCl_2$, 20 mM MOPS, 20% glycerol, 0.25 mM DTT, 0.4 mM ADP, pH of 7.0 was used for titration experiments (see below).

3.3. Functional Assays

3.3.1. SERCA/PLN Co-reconstitution

Lyophilized PLN protein was solubilized in 240 μL of chloroform containing 2.4 mg of lipids in a 4:1 molar ratio of 1,2-dioleoyl-*sn*-glycero-3-phosphocholine (DOPC) and 1,2-dioleoyl-*sn*-glycero-3-phosphoethanolamine (DOPE). Samples were then dried by removing the organic solvent under a stream of N_2 gas. The dried film of lipid and PLN was then hydrated in 120 μL of 25 mM imidazole (pH 7.0) by vortexing followed by brief (30–60 s) water bath sonication. The lipid/PLN vesicles were then adjusted to contain a final concentration of 20 mM imidazole (pH 7.0), 0.1 M KCl, 5 mM $MgCl_2$, and 10% glycerol. 4.8 mg of β-octylglucoside was added, followed by 60 μg of purified SERCA with the final volume adjusted to 300 μL with buffer. Removal of the detergent was performed by incubation with 120 mg of wet Biobeads for 3 h at 25°C. The SERCA/PLN lipid vesicles were separated from Biobeads using a gel-loading tip and micropipette and immediately assayed for function.

3.3.2. ATPase Activity Measurements

SERCA activity was assayed by an enzyme-linked assay (23) performed in a 96-well plate. Each assay was performed at 37°C in a Thermomax microplate reader (Molecular Devices) in triplicate at different free calcium concentrations in a total volume of 175 μL. Between 1 and 3 μg of SERCA was added to the samples to start the assay, and the absorbance of NADH was monitored at 340 nm to determine the rate of ATP hydrolysis. Data were plotted in Origin 7.5 and fit using the Hill equation (see below) to determine the shift in pK_{Ca} (Fig. 1b).

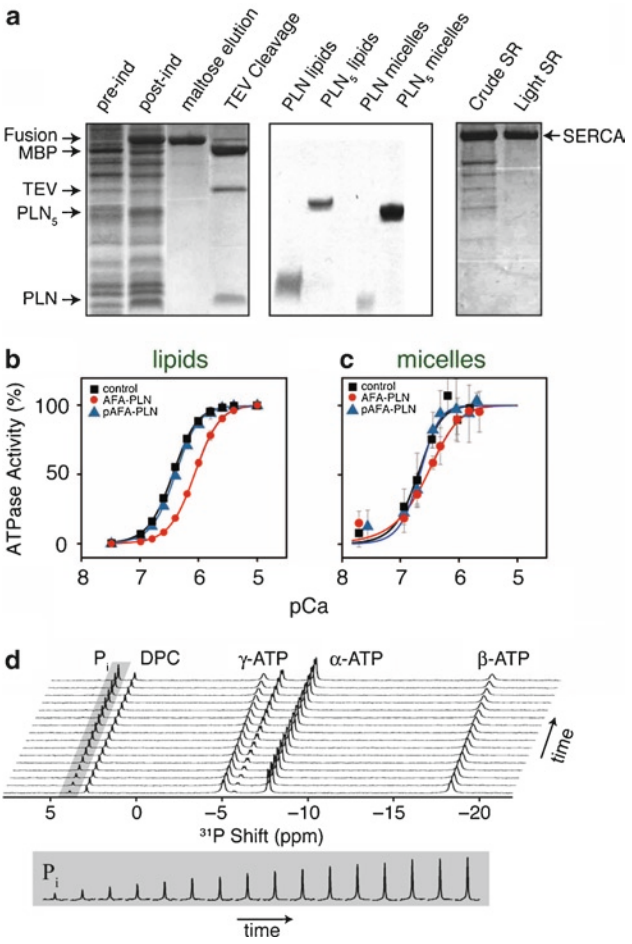

Fig. 1. Purification and functional assays of PLN and SERCA. (**a**) Purification gels showing expression of fusion protein (before and after induction with IPTG), selection on amylose affinity column, and cleavage by TEV protease (*left gel*). *Middle gel* shows PLN monomer and pentamer reconstituted in DOPC/DOPE lipid bilayers and DPC detergent micelles. *Right gel* shows purification of SERCA from crude SR; light SR refers to purified SERCA used for activity assays and NMR experiments. (**b**) Normalized SERCA activity in the absence (*squares*) and presence of PLN (*circles*), and in the presence of phosphorylated PLN at S16 (*triangles*). This activity assay was performed in lipid bilayers using the coupled enzyme assay in a microplate reader. (**c**) SERCA activity monitored using ^{31}P NMR spectroscopy in DPC micelles. (**d**) Example of the ^{31}P NMR activity assay where the inorganic phosphate signal (*highlighted* in *gray*) is monitored as a function of time. *Middle gel* in (**a**) is reproduced with permission from ref. 37 Copyright 2007 National Academy of Sciences, USA. *Panel* (**b**) is reproduced with permission from ref. 19 Copyright 2008 American Chemical Society. *Panels* (**c**, **d**) are reproduced with permission from ref. 18 Copyright 2006 Elsevier.

3.3.3. ^{31}P NMR Activity Assays

To measure the hydrolysis of ATP by SERCA under solution NMR conditions (DPC detergent micelles), assays were performed by monitoring the inorganic phosphate ^{31}P NMR signal. The assay mixture consisted of 6 μM SERCA, 137 μM PLN, assay mix, and concentrations of $CaCl_2$ required to reach free

Ca^{2+} concentration calculated based on the method of Fabiato and Fabiato (24). Upon each addition of nucleotide, eight free induction decays (FIDs) were collected, each consisting of 16 single pulse transients on ^{31}P. Data were collected on a Varian Inova spectrometer operating at a ^{1}H Larmor frequency of 500 MHz (Fig. 1). After monitoring the rate, the inorganic phosphate signal was normalized to the known amount of DPC in the sample. This normalized amount was then plotted (V vs. p_{Ca}) and fit by the Hill equation (Fig. 1c).

$$V = V_{max} / [1 + 10^{n(pK_{Ca} - p_{Ca})}] \quad (1)$$

where V is the initial ATPase rate and n is the Hill coefficient. The data were normalized to the maximal rate, V_{max}, which was obtained from the fit, and then replotted to determine the shift in pK_{Ca} (Fig. 1b).

3.4. NMR Spectroscopy

3.4.1. Preparation of Solution NMR Samples and Titrations

NMR samples were prepared by dissolving isotopically labeled PLN in NMR sample buffer containing 300 mM DPC and 10% D_2O to a final concentration of 0.23 mM. For the preparation of wt-PLN NMR samples (or other "difficult" samples; see Note 3), a slightly different procedure was used: wt-PLN was solubilized in 300 mM DPC, 20 mM PBS (pH 6.0), and 6 M guanidinium–HCl. The sample was dialyzed overnight in a mini-dialysis chamber against 1 L dialysis buffer. For the NMR titration, SERCA at a concentration of 0.51 mM was added incrementally to the PLN sample as previously reported (17). To correct for this dilution, and potential pH and salt effects, the same titration experiment was performed with SERCA buffer in the absence of enzyme. After each SERCA addition, a ^{1}H–^{15}N heteronuclear single quantum coherence (HSQC) experiment was collected on a Varian Inova spectrometer operating with a ^{1}H Larmor frequency of 600 MHz at 37°C, using an inverse detection triple-resonance and triple-axis gradient probe. The HSQC pulse program was equipped with pulsed field gradients for both coherence selection and sensitivity enhancement (25).

3.4.2. K_d Measurements by NMR

For measuring the binding constants, we assumed 1:1 molar ratio between SERCA and PLN, and that the intensity reduction ($I_{retention}$) of the transmembrane domain residues in Fig. 2c was directly related to the fraction of PLN bound to SERCA (f_b). For a complete derivation of Eq. 3 see ref. 18.

$$f_b = 1 - I_{retention} \quad (2)$$

$$f_b = \frac{K_d + [SERCA]_t + [PLN]_t - \sqrt{(K_d + [SERCA]_t + [PLN]_t)^2 - 4[SERCA]_t[PLN]_t}}{2[PLN]_t} \quad (3)$$

The dissociation constant (K_d) was calculated using a nonlinear fit to Eq. 3.

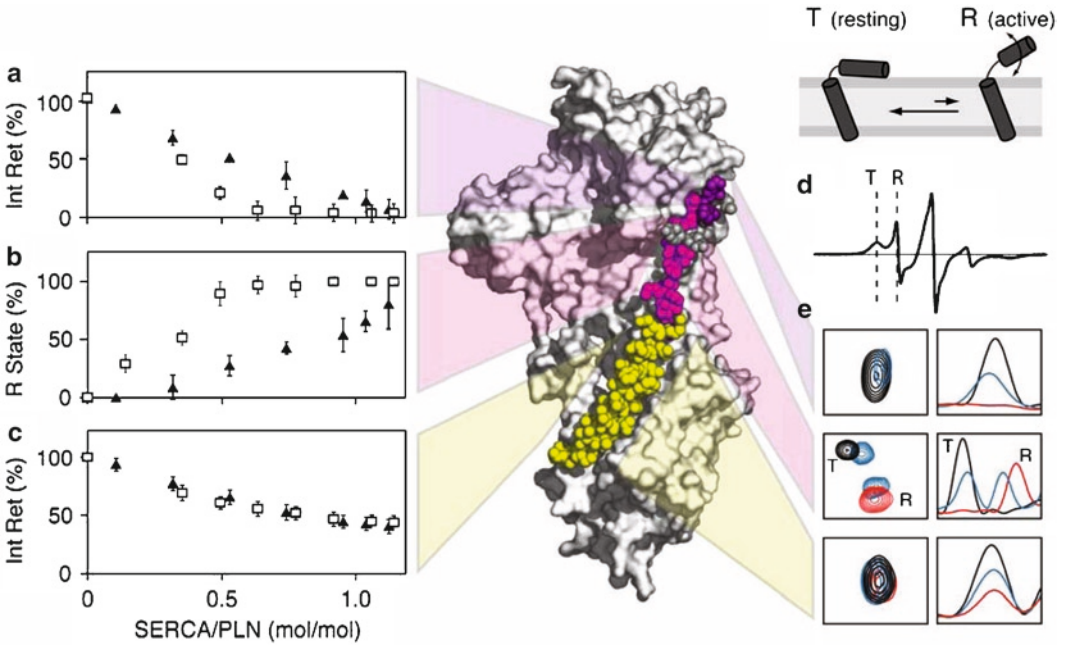

Fig. 2. Solution NMR results on AFA–PLN/SERCA complex in detergent micelles. (**a**) The intensity retention plotted for the T state peaks of residues 2, 3, 6, and 8 in p16 PLN (*white*) and PLN (*black*) that disappear with increasing additions of SERCA. (**b**) The percentage of PLN in the R state as a function of the SERCA/PLN molar ratio for p16 PLN (*white*) and PLN (*black*) for residues undergoing slow exchange (residues 10–12, 15–17, and 22). A value of 100% indicates that the peak (residue) has completely exchanged to the R state. (**c**) The intensity retention for residues in the transmembrane domain (28–52) that decrease, but do not abolish in intensity. (**d**) EPR spectrum of TOAC-labeled A11 PLN in lipid bilayers in the absence of PLN. Since EPR probes a faster timescale, both the T and R states are observed in lipids. (**e**) Representative 1D and 2D spectra of the residues with abolished intensity (*top*, corresponds to **a**), residues undergoing slow exchange (*middle* corresponds to **b**), and residues with reduced intensity (*bottom*, corresponds to **c**). Coordinates for the PLN/SERCA molecular model were generously provided by Drs. MacLennan and Toyoshima. *Panels* (**a**–**c**), and (**e**) were adapted with permission from ref. 18 Copyright 2006 Elsevier. *Panel* (**d**) was reproduced with permission from ref. 17 Copyright 2005 National Academy of Sciences, USA.

3.4.3. Preparation of Oriented Samples and Solid-State NMR Spectroscopy

PLN was reconstituted into lipid vesicles using two different preparations: (1) detergent mediated reconstitution and (2) organic solvent mediated reconstitution.

Detergent mediated reconstitution: 80 mg (4/1, w/w) of DOPC/DOPE were dissolved in chloroform and thoroughly vortexed. Chloroform was evaporated under a stream of N_2, after which the lipids were resuspended in 40 mL of ddH_2O. The lipid suspension was sonicated on ice until small unilamellar vesicles (SUVs) were formed (the suspension became transparent). After sonication, the lipids were centrifuged (6,370 × *g* for 10 min at 4°C) to remove larger vesicles and metal particles. PLN (~4 mg) was solubilized in 1 mL of SDS (10%, w/v), dissolved in the lipid mixture prior, and subjected to one freeze–thaw cycle. Samples were extensively dialyzed against ddH_2O to remove the detergent and subsequently

concentrated to 2 mL using an ultrafiltration device (10 kDa cutoff membrane). Approximately 100 µL of sample was transferred onto each of 20 glass plates. Samples were slowly dried at 40°C, rehydrated, and finally sealed in a rectangular glass cell.

Organic solvent mediated reconstitution: DOPC/DOPE 80 mg (4/1, w/w) were dissolved in chloroform and thoroughly mixed. PLN (~4 mg) was solubilized in 50 µL of trifluoroethanol and added to the lipid mixture. Solvents were first evaporated under a stream of N_2 and then lyophilized overnight to ensure complete removal of organic solvents. The lipid/protein mixture was resuspended in 40 mL of ddH_2O and carefully vortexed. Small unilamellar vesicles were prepared by repeatedly extruding the lipid mixture through polycarbonate filters of decreasing pore size (200, 100, 50 nm) using a bench-top extruder. This SUV suspension was concentrated to 2 mL with samples dried and rehydrated as reported above. The final molar ratio of lipid/protein for all samples was ~200/1.

NMR spectroscopy: The 2D polarization inversion spin exchange at the magic angle (PISEMA) was performed (26, 27) with TPPM decoupling during acquisition (28). A phase modulated Lee-Goldburg (PMLG) sequence was used in the indirect dimension to decouple ^{1}H–^{1}H interactions and allow for the evolution of ^{1}H–^{15}N dipolar coupling (29). The initial 90° ^{1}H pulse, cross-polarization, PMLG (^{1}H effective field), and TPPM decoupling during acquisition were applied at ~60 kHz RF field strength. Spectra of uniformly ^{15}N samples were acquired with 1 k scans and 30t_1 increments, while selectively labeled samples required 4–12 k scans and ~8–16 increments. All experiments were performed at the National High Magnetic Field Laboratory at a 14.1-T magnetic field strength (^{1}H frequency of 600.1 MHz) equipped with a Bruker DMX spectrometer using a low-E probe built by the RF program (30).

3.4.4. Structure Determination of Monomeric PLN Using a Hybrid Solution and Solid-State NMR Method

Solution and solid-state NMR methods have been used as a complementary approach to the structure determination of small and medium-size membrane proteins (31, 32). For solution NMR, the proteins are reconstituted in detergent micelles with a meticulous choice of experimental conditions, which is based on the NMR spectral features as well as preservation of SERCA function. For solid-state, we reconstitute membrane proteins in synthetic lipid bilayers, which are more amenable to enzyme function. The major advantage of solution NMR is to offer high-resolution spectra (membrane proteins up to 100 kDa have now been studied and assigned) and to obtain secondary and tertiary structures through NOE measurements. On the other hand, when membrane proteins are solubilized in detergent micelles, the topological information of the protein within the lipid bilayer is lost.

This orientation information regarding the molecular topology can be recovered by solid-state NMR measurements using aligned samples.

Recent reports verify that several membrane proteins adopt a similar structure in both lipid bilayers and detergent micelles; therefore, we decided to pool the information derived from these two techniques and combine the structural restraints into a unique molecular modeling protocol (33, 34). The total potential energy function (E_{total}) is defined as a combination of an empirical energy function (E_{chem}) and two penalty functions that include solution (E_{solNMR}) and solid-state NMR (E_{ssNMR}) restraints (34):

$$E_{total} = E_{chem} + E_{solNMR} + E_{ssNMR} \quad (4)$$

where

$$E_{chem} = E_{bonds} + E_{angles} + E_{torsion} + E_{improper} + E_{vdw} \quad (5)$$

$$E_{solNMR} = E_{NOEs} + E_{CDIH} + E_{HBOND} + E_{RDC} + E_{PRE} + E_{CSP} \quad (6)$$

$$E_{ssNMR} = E_{CSA} + E_{DC} \quad (7)$$

The energy terms of E_{chem} are included into standard force field of XPLOR-NIH (35). E_{ssNMR} contains dipolar coupling and anisotropic chemical shift values derived from PISEMA or HETCOR experiments. As a result, the simulated annealing protocol minimizes the energy function for both distance and angular restraints as well as orientational restraints derived from solid-state NMR PISEMA experiments. Figure 3d shows the average structures from the lowest energy conformational ensemble for the PLN monomer (33).

3.5. Conclusions

3.5.1. Allosteric Model of SERCA Regulation by PLN

The outcomes of our investigation are summarized within the schematic in Fig. 4. In agreement with both in vitro and in vivo studies, we found that PLN adopts a pentameric, L-shaped conformation both in micelles and in lipid bilayers. In particular, both solution and solid-state NMR data show that the cytoplasmic domain (which is amphipathic) interacts with the surface of the membrane-mimicking environment (both for micelles and lipid bilayers), while the transmembrane domain forms a tight hydrophobic bundle stapled together by a leucine–isoleucine zipper. PLN depolymerization into active monomers occurs in the presence of SERCA. In the monomeric state (prelude to the interaction with SERCA), PLN is predominantly in a resting T state with a small population in the R state. Using EPR spectroscopy, Thomas and co-workers have estimated that ~16% of PLN exists in the R state in lipid bilayers at 4°C (13). In the presence of SERCA, the equilibrium

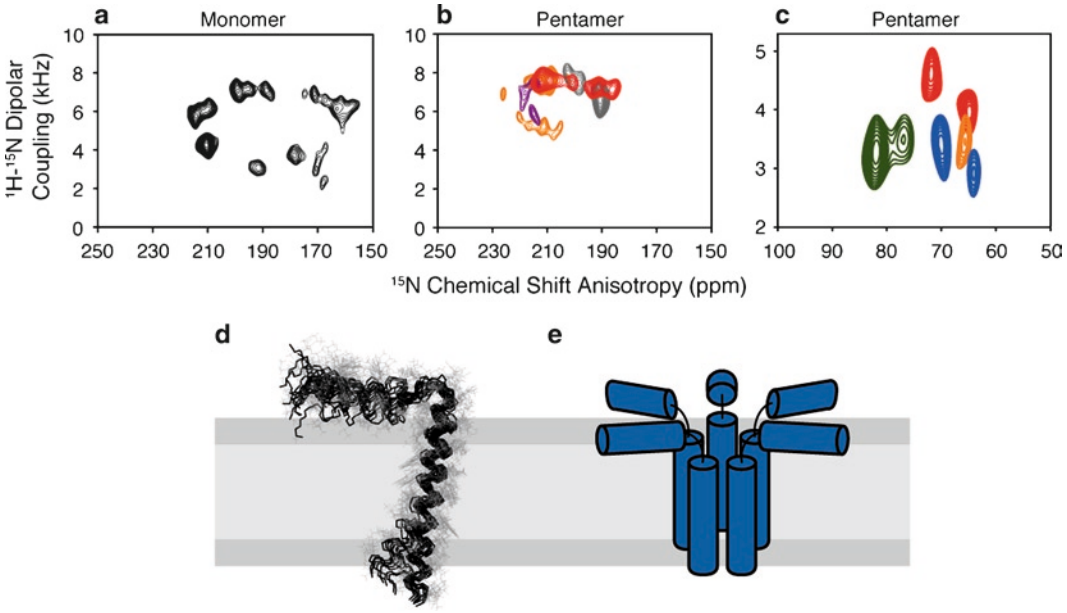

Fig. 3. Solid-state NMR spectra with overlaid ensemble PLN structures. PISEMA spectra for uniformly ^{15}N-labeled PLN monomer (**a**) and selectively labeled PLN pentamer ((**b**) transmembrane domain residues and (**c**) cytoplasmic domain residues). Note that dipolar coupling values within the spectra are scaled by the theoretical 0.82 factor for the PISEMA experiment (26). *Panel* (**d**) shows the overlay of the structural ensemble for monomeric PLN determined using a hybrid of solution and solid-state NMR restraints (*PDB* 2KB7) (33). *Panel* (**e**) shows a *cartoon* representation of the PLN pentamer indicating the pinwheel assembly (37). *Panels* (**a**–**c**) are reproduced with permission from refs. 33, 37. Copyright 2007 and 2009 National Academy of Science, USA.

is shifted toward the R state that is probably selected to bind the enzyme. While this initial detection of PLN ground (T) and excited (R) states shed light into the dynamic regulatory process of SERCA, more experiments are needed to characterize the excited states both structural and dynamically. Our ongoing investigation is revealing a more complex equilibrium than previously anticipated. Although dynamic in nature, PLN forms a stable inhibitory complex with SERCA (K_d in DPC detergent micelles ~60 μM). This inhibition is reversed by phosphorylation at S16, which changes the conformational dynamics and results in a partial unwinding of the cytoplasmic helix (20). In the presence of SERCA, phosphorylation at S16 PLN causes a slight rearrangement within domain Ib (residues 23–30) and changes the dynamics at the binding interface (13, 18). These structural dynamics affect the conformational transitions of the enzyme, and ultimately calcium translocation.

3.5.2. Rational Design of PLN Mutants as Possible Candidates for Gene Therapy

A fundamental aim of structural biology is to move from understanding structure and dynamics to controlling molecular function. With this in mind, we attempted to manipulate the structural dynamics of PLN and to promote the formation of the R state

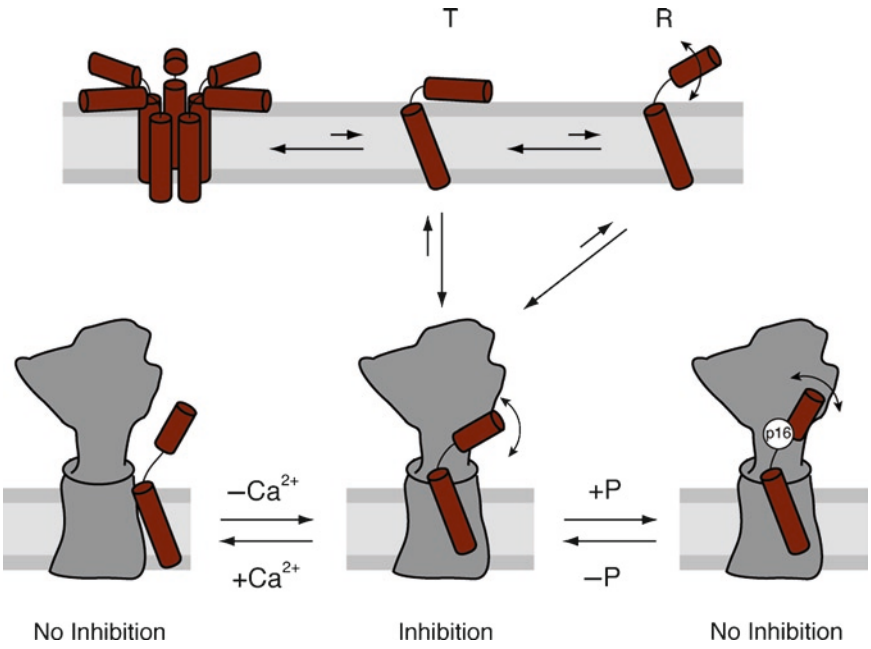

Fig. 4. Allosteric model of PLN/SERCA interaction showing depolymerization of pentameric PLN into monomeric units that undergo exchange between an ordered T state and a disordered R state(s) (11, 13, 17–19).

through mutagenesis. Recently, we found that by mimicking the S16 phosphorylated state of PLN (i.e., enhancing the local dynamics in the hinge region), it is possible to tune the extent of SERCA inhibition (36). This work was originally inspired by in vivo studies carried out by Chien and co-workers, who demonstrated that a pseudo-phosphorylated variant of PLN can relieve SERCA inhibition and increase heart contractility, ultimately reversing the damages of myocardial infarction. We found that by changing Pro21 to Gly it is possible to generate a *loss-of-function* mutant with characteristics similar to S16E (pseudo-phosphorylated species tested by Chien), preserving the posttranslational control by β-adrenergic stimuli (36). This new generation of mutants possesses a *residual inhibitory power* that could be important in adjusting the pathophysiology of diseased hearts leading to reversal or hindrance of cardiac remodeling. We are currently working on different sites to improve the characteristics of *loss-of-function* mutants.

4. Notes

1. For small membrane peptides, choice of fusion partner and cleavage protease can be crucial for successful expression and purification. Expression of small membrane peptides can

induce the formation of inclusion bodies, or lead to cell death. We attempted cloning PLN with several fusion partners and found MBP to offer the best degree of solubility and expression levels. For choosing a cleavage protease, scanning for secondary cleavage sites is also very important. For PLN, cleaving with thrombin and other proteases led to secondary cleavage. TEV has a longer recognition sequence (seven residues), making it very specific.

2. TEV can be easily expressed in *E. coli* and purified using a 6× His and Ni-NTA resin chromatography within the laboratory. A construct of TEV that is particularly effective which we use is a S219V mutant with a poly-arginine tail kindly provided to us by the Gorelick Laboratory.
3. The method of unfolding the protein sample with guanidine-HCl and refolding via dialysis used to prepare the wt-PLN solution-state NMR samples described in Subheading 3.4.1 is useful for other membrane protein NMR samples that are prone to aggregation or those which give nonuniform HSQC spectra. We have found that other "difficult" samples (such as pS16 PLN) give better spectra when prepared in this manner.

Acknowledgment

This work was supported by grants to GV from the National Institutes of Health (GM64742, HL80081, GM072701) and NJT (AHA 0515491Z). PISEMA spectra were acquired at the NHMFL, Tallahassee, FL (DMR-0084173). NMR instrumentation at the University of Minnesota High Field NMR Center was funded by the National Science Foundation (BIR-961477) and the University of Minnesota Medical School.

References

1. Mac Lennan DH, Kranias EG (2003) Phospholamban: a crucial regulator of cardiac contractility. Nat Rev 4:566–577
2. Kranias EG, Bers DM (2007) Calcium and cardiomyopathies. Subcell Biochem 45:523–537
3. Hoshijima M, Knoll R, Pashmforoush M, Chien KR (2006) Reversal of calcium cycling defects in advanced heart failure toward molecular therapy. J Am Coll Cardiol 48:A15–A23
4. Inesi G, Lewis D, Ma H, Prasad A, Toyoshima C (2006) Concerted conformational effects of Ca^{2+} and ATP are required for activation of sequential reactions in the Ca^{2+} ATPase (SERCA) catalytic cycle. Biochemistry 45:13769–13778
5. Toyoshima C, Inesi G (2004) Structural basis of ion pumping by Ca^{2+}-ATPase of the sarcoplasmic reticulum. Annu Rev Biochem 73:269–292
6. Toyoshima C, Nakasako M, Nomura H, Ogawa H (2000) Crystal structure of the calcium pump of sarcoplasmic reticulum at 2.6 Å resolution. Nature 405:647–655
7. Inesi G, Prasad AM, Pilankatta R (2008) The Ca^{2+} ATPase of cardiac sarcoplasmic reticulum: physiological role and relevance to diseases. Biochem Biophys Res Commun 369:182–187
8. Negash S, Chen LT, Bigelow DJ, Squier TC (1996) Phosphorylation of phospholamban

by cAMP-dependent protein kinase enhances interactions between Ca-ATPase polypeptide chains in cardiac sarcoplasmic reticulum membranes. Biochemistry 35:11247–11259

9. Negash S, Sun H, Yao Q, Goh SY, Bigelow DJ, Squier TC (1998) Cytosolic domain of phospholamban remains associated with the Ca-ATPase following phosphorylation by cAMP-dependent protein kinase. Ann N Y Acad Sci 853:288–291
10. Negash S, Yao Q, Sun H, Li J, Bigelow DJ, Squier TC (2000) Phospholamban remains associated with the Ca^{2+}- and Mg^{2+}-dependent ATPase following phosphorylation by cAMP-dependent protein kinase. Biochem J 351:195–205
11. Mueller B, Karim CB, Negrashov IV, Kutchai H, Thomas DD (2004) Direct detection of phospholamban and sarcoplasmic reticulum Ca-ATPase interaction in membranes using fluorescence resonance energy transfer. Biochemistry 43:8754–8765
12. Kirby TL, Karim CB, Thomas DD (2004) Electron paramagnetic resonance reveals a large-scale conformational change in the cytoplasmic domain of phospholamban upon binding to the sarcoplasmic reticulum Ca-ATPase. Biochemistry 43:5842–5852
13. Karim CB, Zhang Z, Howard EC, Torgersen KD, Thomas DD (2006) Phosphorylation-dependent conformational switch in spin-labeled phospholamban bound to SERCA. J Mol Biol 358:1032–1040
14. Thomas DD, Reddy LG, Karim CB et al (1998) Direct spectroscopic detection of molecular dynamics and interactions of the calcium pump and phospholamban. Ann N Y Acad Sci 853:186–194
15. Stokes DL, Green NM (1990) Three-dimensional crystals of CaATPase from sarcoplasmic reticulum. Symmetry and molecular packing. Biophys J 57:1–14
16. Stokes DL, Pomfret AJ, Rice WJ, Glaves JP, Young HS (2006) Interactions between Ca^{2+}-ATPase and the pentameric form of phospholamban in two-dimensional co-crystals. Biophys J 90:4213–4223
17. Zamoon J, Nitu F, Karim C, Thomas DD, Veglia G (2005) Mapping the interaction surface of a membrane protein: unveiling the conformational switch of phospholamban in calcium pump regulation. Proc Natl Acad Sci U S A 102:4747–4752
18. Traaseth NJ, Thomas DD, Veglia G (2006) Effects of Ser16 phosphorylation on the allosteric transitions of phospholamban/Ca(2+)-ATPase complex. J Mol Biol 358: 1041–1050
19. Traaseth NJ, Ha KN, Verardi R et al (2008) Structural and dynamic basis of phospholamban and sarcolipin inhibition of Ca(2+)-ATPase. Biochemistry 47:3–13
20. Metcalfe EE, Traaseth NJ, Veglia G (2005) Serine 16 phosphorylation induces an order-to-disorder transition in monomeric phospholamban. Biochemistry 44:4386–4396
21. Buck B, Zamoon J, Kirby TL et al (2003) Overexpression, purification, and characterization of recombinant Ca-ATPase regulators for high-resolution solution and solid-state NMR studies. Protein Expr Purif 30:253–261
22. Douglas JL, Trieber CA, Afara M, Young HS (2005) Rapid, high-yield expression and purification of Ca^{2+}-ATPase regulatory proteins for high-resolution structural studies. Protein Expr Purif 40:118–125
23. Madden TD, Chapman D, Quinn PJ (1979) Cholesterol modulates activity of calcium-dependent ATPase of the sarcoplasmic reticulum. Nature 279:538–541
24. Fabiato A, Fabiato F (1979) Calculator programs for computing the composition of the solutions containing multiple metals and ligands used for experiments in skinned muscle cells. J Physiol 75:463–505
25. Kay LE, Keifer E, Saarinen T (1992) Pure absorption gradient enhanced heteronuclear single quantum correlation spectroscopy with improved sensitivity. J Am Chem Soc 114:10663–10665
26. Wu CH, Ramamoorthy A, Opella SJ (1994) High-resolution heteronuclear dipolar solid-state NMR spectroscopy. J Magn Reson 109:270–272
27. Ramamoorthy A, Wei Y, Lee D (2004) PISEMA solid-state NMR spectroscopy. Annu Rep NMR Spectrosc 52:1–52
28. Bennett AE, Rienstra CM, Auger M, Lakshmi KV, Griffin RG (1995) Heteronuclear decoupling in rotating solids. J Chem Phys 103:6951–6958
29. Vinogradov E, Madhu PK, Vega S (1999) High-resolution proton solid-state NMR spectroscopy by phase-modulated Lee–Goldburg experiment. Chem Phys Lett 314:443–450
30. Gor'kov PL, Chekmenev EY, Li C et al (2007) Using low-E resonators to reduce RF heating in biological samples for static solid-state NMR up to 900 MHz. J Magn Reson 185:77–93
31. Opella SJ, Marassi FM (2004) Structure determination of membrane proteins by NMR spectroscopy. Chem Rev 104:3587–3606
32. Gao FP, Cross TA (2005) Recent developments in membrane–protein structural genomics. Genome Biol 6:244

33. Traaseth NJ, Shi L, Verardi R, Mullen DG, Barany G, Veglia G (2009) Structure and topology of monomeric phospholamban in lipid membranes determined by a hybrid solution and solid-state NMR approach. Proc Natl Acad Sci U S A 106: 10165–10170
34. Shi L, Traaseth NJ, Verardi R, Cembran A, Gao J, Veglia G (2009) A refinement protocol to determine structure, topology, and depth of insertion of membrane proteins using hybrid solution and solid-state NMR restraints. J Biomol NMR 44:195–205
35. Schwieters CD, Kuszewski JJ, Tjandra N, Clore GM (2003) The Xplor-NIH NMR molecular structure determination package. J Magn Reson 160:65–73
36. Ha KN, Traaseth NJ, Verardi R et al (2007) Controlling the inhibition of the sarcoplasmic Ca^{2+}-ATPase by tuning phospholamban structural dynamics. J Biol Chem 282:37205–37214
37. Traaseth NJ, Verardi R, Torgersen KD, Karim CB, Thomas DD, Veglia G (2007) Spectroscopic validation of the pentameric structure of phospholamban. Proc Natl Acad Sci U S A 104:14676–14681